Field survey of the 2017 Typhoon Hato and a comparison with storm surge modeling in Macau

Linlin Li[1*], Jie Yang[2,3*], Chuan-Yao Lin[4], Constance Ting Chua[5], Yu Wang[1,6], Kuifeng Zhao[2], Yun-Ta Wu[2], Philip Li-Fan Liu[2,7,8], Adam D. Switzer[1,5], Kai Meng Mok[9], Peitao Wang[10], Dongju Peng[1]

[1]Earth Observatory of Singapore, Nanyang Technological University, Singapore

[2]Department of Civil and Environmental Engineering, National University of Singapore, Singapore

[3]College of Harbor, Coastal and Offshore Engineering, Hohai University, China

[4]Research Center for Environmental Changes, Academia Sinica, Taipei 115, Taiwan

[5]Asian School of the Environment, Nanyang Technological University, Singapore

[6]Department of Geosciences, National Taiwan University, Taipei, Taiwan

[7]School of Civil and Environmental Engineering, Cornell University, USA

[8]Institute of Hydrological and Ocean Research, National Central University, Taiwan

[9]Department of Civil and Environmental Engineering, University of Macau, Macau, China

[10]National Marine Environmental Forecasting Center, Beijing, China

Corresponding to: Linlin Li (llli@ntu.edu.sg) ; Jie Yang (jie_yang@hhu.edu.cn)

Abstract: On August 23, 2017 a Category 3 Typhoon Hato struck Southern China. Among the hardest hit cities, Macau experienced the worst flooding since 1925. In this paper, we present a high-resolution survey map recording inundation depths and distances at 278 sites in Macau. We show that one half of the Macau Peninsula was inundated with the extent largely confined by the hilly topography. The Inner Harbor area suffered the most with the maximum inundation depth of 3.1m at the coast. Using a combination of numerical models, we simulate and reproduce this typhoon and storm surge event. We further investigate the effects of tidal level and sea level rise on coastal inundations in Macau during the landfall of a 'Hato like' event.

1 Introduction

On August 23, 2017, at approximately 12:50 pm local time Typhoon Hato made landfall near Zhuhai, which is located on the Southern coast of Guangdong province, China (Figure 1). With an estimated 1-minute sustained wind speed of 185 km/h near its center and a minimum central pressure of 945 hPa, Typhoon Hato was a Category 3

28   Hurricane on the Saffir-Simpson scale. Typhoon Hato was one of the strongest typhoons to affect the coastal areas

29   of the Pearl River Estuary (PRE) in Southern China over the last several decades. It caused widespread coastal

30   flooding in the PRE areas (ESCAP/WMO Typhoon Committee, 2017). Major cities in the northeast quadrant of the

31   typhoon track, including Macau, Zhuhai and Hong Kong, were severely affected. The resulting maximum storm

32   surge heights (water level above the astronomical tide) reached 1.62 m at A-Ma station in Macau, the highest since

33   water level recording began in 1925. Elsewhere in the PRE areas, a maximum storm surge of 2.79 m was recorded at

34   Zhuhai, and 1.18m, 1.65m and 2.42 m at Quarry Bay, Tai Po Kau and Tsim Bei Tsui in Hong Kong, respectively

35   (HKO, 2017) (Figure 1b). The extreme flooding in Macau was historically unprecedented in terms of the inundation

36   depth as well as the extent, and more than half of the Macau Peninsula was inundated. Typhoon Hato's strong wind

37   and the associated flooding resulted in 22 fatalities and caused 3.5 billion USD direct economic losses (Benfield,

38   2018).

39   Macau (and Hong Kong) commonly experience about 5-6 typhoons per year (Lee et al., 2012) and as the result the

40   low-lying area in the western part of Macau Peninsula has been frequently flooded by storm surges during major

41   typhoons. Relatively recent typhoons such as Becky (1993), Hagupit (2008), Koppu (2009), and Vicente (2012) all

42   generated storm surges that produced maximum inundation depths > 1 m in Macau, while the unnamed historical

43   typhoons in 1927 and 1948, and typhoon Gloria (1957) generated storm surges > 1.15 m (see the historical flood

44   records http://www.smg.gov.mo/smg/database/e_stormsurge_historicalRec.htm). Although frequently affected by

45   storm surges, the extreme inundation brought by Typhoon Hato still caught Macau unprepared. Consequently, the

46   local government has declared Typhoon Hato as the "worst-case" scenario and will use it as a criterion for designing

47   new engineering measures for coastal protection.

48   While Typhoon Hato has caused the worst flood event in Macau's history, the key flood parameters (e.g. the water

49   depth and inundation distance) have not been properly documented. Although, Macau has 2 tidal gauge stations and

50   17   inland   water   gauge   stations   distributed   in   the   areas   susceptible   to   flooding

51   (http://www.smg.gov.mo/smg/ftgms/e_ftgms.htm). Unfortunately, they all failed to record the peak water level due

52   to breakdown or electricity interruption of devices during Hato (SMG, 2017). Therefore, post event surveys of key

53   flood parameters become essential for better understanding storm surge dynamics and inundation characteristics

54   (e.g. Fritz et al., 2007;Tajima et al., 2014;Takagi et al., 2017;Soria et al., 2016). For this reason, our field survey

55   team was deployed to Macau and Zhuhai on August 26, 2017 and collected flood and damage information for 5

56   days. Here, the survey data have been analyzed and used to produce a high-resolution inundation map of Macau.

57   Qualitatively speaking, several factors have contributed to the exceptional damage during Typhoon Hato: 1)

58   Typhoon Hato occurred during the second day of a Lunar month and the landfall time roughly coincided with the

59   astronomical high tide; 2) According to the record, Typhoon Hato's wind speed was the strongest among all the

60   typhoons in Macau since 1953. The peak wind gust reached 217.4 km/h in Taipa Grande station and broke the

61   record of 211.0 km/h set by Typhoon Ruby in 1964 (SMG, 2017;Shan et al., 2018). 3) The translation wind speed of

62   Typhoon Hato exceeded 30 km/h (Takagi et al., 2018) before its landfall, which is unusually high compared with the

63   average transitional speed of 10-15 km/h in the South China Sea (Shan et al., 2018). 4) According to Hong Kong

64   Observatory, Typhoon Hato momentarily became a super typhoon during its approach towards the Pearl River

65   Estuary in the morning of August 23 (HKO, 2017). The sudden intensification occurred because of the low vertical

66   wind shear and the high sea surface temperature of ~31 °C in the Northern portion of the SCS (HKO, 2017).

67   It is well-known that the tide during a typhoon's landfall plays a significant role in the severity of the storm surge

68   induced inundation. In the case of Typhoon Hato, the coincidence of astronomical high tide and the landfall time is

69   thought to be the major factor causing the wide-spread flooding in Macau. However, using the OSU TPXO-atlas8

70   tide model (Egbert and Erofeeva, 2002) and the tide gauge location (113.551 ° E 22.167 ° N) in Macau, we

71   estimated the peak tidal level on the day of Hato's landfall occurred at 10:00 AM on August 23, 2017 with the tide

72   level of 0.927 m above the mean sea level (MSL), while the estimated tidal level was only 0.470 m above the MSL

73   at the reported Typhoon Hato's landfall time around 12:50 pm on August 23, 2017. Thus, Typhoon Hato actually

74   made landfall almost 3 hours after the peak tidal level, while the tidal level differences are almost 0.5 meter. Thus,

75   it is intriguing to ask what if Typhoon Hato had occurred at a different time with a lower or higher tidal level, how

76   would the inundation areas change?

77   To provide a quantitative answer for the question posted above, a numerical simulation tool must be validated first.

78   In this paper, the tide-surge-wave coupled hydrodynamic model, SCHISM (Semi-implicit Cross-scale Hydroscience

79   Integrated System Model) (Zhang et al., 2016) is combined with the Weather Research and Forecasting (WRF)

80   model (Skamarock et al., 2008) to simulate the entire Typhoon Hato event. The high-resolution bathymetric data in

81   PRE and topographic data in Macau are employed for calculating coastal flooding. Model-data comparisons are

82   performed to ensure that the wind fields are reproduced well by the WRF model. The field survey data (e.g.

83   inundation depth and area) are used to check the accuracy of the storm surge model. Once the numerical model is

84   validated, we can use it to conduct a series of numerical experiments to assess the possible impact of 'Hato-like'

85   typhoon occurring at different tidal levels. Then looking at such hazard event and its counter-measures from a long-

86   term perspective, we examined the effect of sea level rise (SLR) on the inundation areas.

87   The paper is presented in the following order. We first report a high-resolution inundation map of Macau based on

88   our field measurements and observations. Then we describe each component of the numerical simulation package

89   followed by the simulation results of Typhoon Hato. Finally, we discuss the effect of tidal level and SLR through the

90   results of numerical experiments.

91   **2 Post-typhoon field survey**

92   On August 26, 2017, three days after Typhoon Hato made landfall, our survey team arrived at Macau, where they

93   surveyed ~ 300 sites in Macau Peninsula, measuring flow depths (water depth above the street level), maximum

94   runup, and inundation distances (Table S1). The team also recorded building damage. The team was able to conduct

95   interviews with many shopkeepers, homeowners and security officers, who witnessed this flood event. The

96   maximum inundation depths were mainly determined by using watermarks as indicators and where possible

97   confirmed by eyewitnesses. Watermarks identified on glass panels, iron gates and light colored walls were

98   photographed (Figure 2) and located using GPS. Inundation extent was determined by tracing watermarks from the

99   coastline to the inundation limit along streets perpendicular to the coastline. Distances between two surveyed sites

100   were about 20 - 25 m apart to ensure the high resolution of this survey map. In total, 278 inundation depths were

101   recorded and eyewitnesses confirmed 96 (35%) of them (Table S1).

102   Figure 3a shows the surveyed inundation depths on the Macau Peninsula. Names of the locations are marked on a

103   high-resolution bare ground elevation map in Figure 3b. The Inner Harbor area, which starts from the A-Ma Temple

104   in the southwest and ends at Qingzhou in the northwest of Macau Peninsula, was completely flooded to a depth of

105   3.1 m at Ponte Pou Heng (the purple dot in Fig 3a). Along the coastal roads of the Inner Harbor, inundation depth

106   reached 2.0 - 2.5m in many low-lying places. When tracing the watermarks along the two major streets: Avenida de

107   Almeida Ribeiro and Ruo Do Gamboa, we observe that, as the seawater penetrated inland, the inundation depth

108   gradually decreased from > 2 m to ~1 m (Fig 3c-d). The inundation extent was clearly confined by the hilly

109   topography (Figure 3a-b). From south to north, the steep topography of the local hills acted as natural barriers,

110   limiting flood propagation. In contrast, the relatively flat (2-3 m above mean sea level) northwest area surrounding

111   "Fai Chi Kei", experienced inundation distances of up to ~1.3 km inland (Figure 3a-b). The coastal area in the

112   northeast was largely spared due to the seawall protection and slightly higher elevation, while the southeast coastal

113   area was slightly flooded by less than 1 m surge with limited inundation distance (<50 m). Considering the size of

114   the Macau Peninsula, which is ~3 km E-W and ~4 km N-S, nearly half of the peninsula was inundated during

115   Typhoon Hato (Figure 3a).

116   Notably, many eyewitnesses commented that this flooding event was characterized by rapid-rising speed;

117   shopkeepers in the Inner Harbor area stated that seawater rose quickly from the ankle level to chest high in less than

118   20 minutes, leaving them no time to rescue property or possessions on the ground floor. The ground-floors of most

119   of buildings in Macau are used for commercial purpose, which partly explains why Macau had suffered from

120   economic loss exceeding 1.42 billion USD (HKO, 2017). Although residents who live in the Inner Harbor area are

121   experienced in battling chronic flooding caused by storm surges, the extreme flood caused by Typhoon Hato still

122   came as a surprise for them in many ways (e.g. its speed, depth and extent). In one of the interviews, an elderly

123   resident who lives on the street of Rua Do Camboa used the length of his body as a yardstick to describe the height

124   of floodwater from previous events. He explained that Typhoon Becky (1993) had resulted in approximately 1.4

125   m floodwater at where he lives; 1.2 m during Typhoon Hagupit (2008); 0.3 m during Typhoon Vicente (2012); and

126   this time Typhoon Hato had resulted in a 2.1 m flood height.

127   The survey data presented in this study is complementary to the data provided by an earlier study (Takagi et al.,

128   2018) in terms of the number of surveyed locations and spatial coverage. Takagi et al. (2018) provided 12 data

129   points in Macau and Hong Kong while our 278 data points are concentrated in Macau with the purpose of

130   constructing a measured high-resolution inundation map. Such map provides not only valuable documentation of

131   such rare and extreme event but also validation data for numerical modelers.

3 Numerical simulation

The WRF model (version 3.8.1) (Skamarock et al., 2008) is used to generate the wind and pressure fields of Typhoon Hato. The initial and meteorological boundary conditions for WRF were obtained from the National Center for Environmental Prediction (NCEP) Global Forecast System (GFS) with $0.5° × 0.5°$ analysis data sets at 6-h interval. The time-varying sea surface temperature (SST) was obtained from $0.5°$ NCEP real-time-global data set. The planetary boundary layer of the Yonsei University boundary layer scheme (Hong et al., 2006) was used with the revised MM5 similarity surface layer scheme (Jiménez et al., 2012) and the unified Noah land surface model (Tewari et al., 2004) over land. The single-moment five-class microphysics scheme (Hong et al., 2004), the updated Kain-Fritsch scheme (Kain, 2004) with a moisture-advection based trigger function (Ma and Tan, 2009), the Rapid Radiation Transfer Model for Global Circulation Models (RRTMG) shortwave and longwave schemes (Iacono et al., 2008) are also adopted in this study. The horizontal resolution of the model is 3 km and the grid box had $921 ×$ 593 points in both east-west and north-south directions. There were 45 vertical levels with the lowest level approximately 50 m above the surface. The output time interval of wind and pressure fields is 10 minutes.

The output wind and pressure fields from the WRF results are then used to drive the storm surge simulation in the tide-surge-wave coupled hydrodynamic model SCHISM (Zhang et al., 2016), which is a derivative code of the original SELFE (Semi-implicit Eulerian-Lagrangian Finite Element) model. The SCHISM system has been extensively tested against Standard Ocean/coastal benchmarks and applied to several regional estuaries for storm-surge inundation modeling (Krien et al., 2017;Wang et al., 2014). In this study, the model is used in the 2DH barotropic mode, which solves nonlinear shallow water equations on unstructured meshes for storm surges. To track the coastline movements, the model includes an efficient wetting-drying algorithm by using semi-implicit time stepping and Eulerian-Lagrangian method for advection (Zhang and Baptista, 2008).

The bottom shear stress is modeled by the Manning's formula with the Manning coefficient being set to 0.025 for the inland area (area above mean sea level) and 0.01 for the offshore area. The values of Manning coefficient are informed by previous studies (e.g. Martyr et al., 2013;Garzon and Ferreira, 2016). We choose relatively low Manning value for the estuary and open sea area as the sediment in the Pearl River Estuary is dominated by very fine sand (mainly silt clays) (Jiang et al., 2014). The drag coefficient for the surface wind stress is computed according to Pond and Pickard (1998). The model is forced by applying tidal elevation series on nodes along open ocean boundaries, which are extracted from the OSU TOPEX/Poseidon Global Inverse Solution model TPXO8-atlas (Egbert and Erofeeva, 2002).

To capture the effects of wind waves in the storm surge simulation, the spectral Wind Wave Model (WWMIII) is employed. WWMIII solves the wave action equations in the frequency domain on the same unstructured grid as SCHISM. Physical processes including wave growth and energy dissipation due to whitecapping, nonlinear interaction in deep and shallow waters, and wave breaking are all considered in the simulations. The WWMIII is dynamically coupled with SCHISM every 600 seconds. The radiation stress is estimated according to (Roland,

166 2008) based on the directional spectra itself. The radiation stresses computed in WWMIII are transferred to
167 SCHISM at each step to update water level and velocity, which are sent as feedback reversely.

168

169 For Typhoon Hato, the simulation domain covers the northern part of the South China Sea (Figure 4a). We create an
170 unstructured grid with horizontal resolution varying from 50 km in the deep sea, ~ 1 km over the shelf to ~ 20 m in
171 the vicinity of Macau (Figure 4b-c). To ensure the accuracy and reliability of the simulation results, we integrated as
172 many available topographic and bathymetric data as possible: 1) The bathymetric data in the Pearl River Estuary are
173 integrated from 36 nautical charts with scales ranging from 1:5000 to 1:250000; 2) high resolution topographic data
174 for Macau is purchased from the Macau Cartography and Cadastre Bureau; 3) 1-arc Shuttle Radar Topography
175 Mission (SRTM) data covering the Pearl River Delta; (c) 5m elevation is specified for the two artificial islands in
176 the eastern side of Macau Peninsula, which are still under construction. The topographic and bathymetric data were
177 complemented by 30 arc seconds General Bathymetric Chart of the Oceans (GEBCO) data and integrated into one
178 dataset after being adjusted to the mean sea level (MSL). Using this model setting, we validated the tidal current
179 model performs well when comparing the simulated tidal cycle with measured data from 1 Nov 2014 to 30 Nov
180 2014 (Figure S1).

181 **4 Results**

182 **4.1 Simulation results of Typhoon Hato**

183 We first compare the wind speeds generated by WRF with the measured data at 9 selected wind gauge stations in the
184 PRE (Figure 5c-k), including 4 local wind gauges in Macau (see the gauge locations in Figure 5a-b). The model/data
185 comparison shows that the WRF model captures Typhoon Hato's wind fields well in terms of both the peak wind
186 speed and the phase (Figure 5c-k).

187 The simulated maximum surge heights in the PRE (Figure 6a) show that the storm surge heights on both sides of the
188 PRE varied widely, ranging from 0 m to 4.5 m. Surge heights > 2.5 m occurred on much of the western side of PRE
189 including Macau. Wave amplification effects, the funnel-shaped coastline in the PRE also likely led to larger surge
190 heights in the inner estuary area. To validate the numerical results, we compare the simulated storm-tides with the
191 measured storm-tides at 4 selected locations (Figure 6b). Very reasonable agreements are observed, ensuring the
192 reliability of the modelling approach used in this study.

193 We further compare the simulated and measured inundation maps in Macau (Figure 6c). The calculated inundation
194 depths are slightly lower (~10%) than the measured ones in some locations near the coastline of "Fai Chi Kei" and
195 southern Inner Harbor and several inland locations in Inner Harbor (see the locations in Figure 3b). The
196 underestimation is likely the by-product of the bare-ground topographic data used in the simulation, which does not
197 include buildings, and hence excludes complex flow patterns (e.g. wave front colliding with buildings) and
198 channeling effects, which locally increase water depth. Nevertheless, the overall agreement is quite good. It

199 demonstrates that the coupled model can reproduce this flood event reasonably well in terms of both inundation
200 depth and extent.

201 In Figure 6d we also plot the simulated arrival time of wave front, which can be viewed as the arrival time of the
202 surge. During Typhoon Hato the surge wave arrived in the southern Inner Harbor first at the local time around
203 11:20 on August 23, 2017 and then propagated eastward inland and northward in the Fai Chi Kei direction in the
204 next one and half hours. The flow velocity was less than 0.5 m/s in the southern Inner Harbor due to the generally
205 steep slope, while in the area surrounding Fai Chi Kei, the flow velocity was faster and was up to 0.7 - 0.8 m/s.
206 When comparing with the 2 – 5 m/s tsunami flow velocity recorded in the Banda Aceh during the 2004 Indian
207 Ocean tsunami (Fritz et al., 2006), the 0.5-0.8 m/s flow velocity of storm tide in Macau is significantly smaller. The
208 information like this demonstrates that numerical model and field survey can complement each other and recover a
209 comprehensive view of disaster scene.

210 **4.2 The effects of tidal level**

211 Having checked our numerical model with measured data and demonstrated that the model can replicate events like
212 Typhoon Hato, we now investigate the effects of tidal level on coastal flooding. Most the PRE including Macau has
213 a mixed semidiurnal tidal cycle in which the semidiurnal lunar tide, M2, is the predominant component followed by
214 K1, O1 and S2. The maximum tidal range observed in Macau is 2.86 m while the difference between mean high
215 water (MHW) and mean low water (MLW) is 1.11 m (calculated from the tide record during 1985-2012).

216 To quantitatively investigate the impact of tidal level at Hato's landfall, we first selected two extreme tidal levels
217 from the years of 1964-2017 using OSU TPXO-atlas8 tide model. The reason we use more extreme tidal levels is
218 because scenarios under those tidal levels can provide the upper and lower bounds of the potential inundations, thus
219 better demonstrating the effect of tidal level. On the other hand, we observe the peak tidal level on the day of
220 Typhoon Hato's landfall was only moderately high compared with the daily higher high water records (HHW) in
221 Macau (Figure S2) although it was the third highest during that month. Putting this peak tide of 0.927 m in all the
222 estimated daily HHW, we can see that this value is lower than 21% of the daily HHW during 1964-2017 (Figure S2
223 shows the HHW and LLW during 2008-2017 as an example). We find the corresponding highest extreme tide
224 (HET) and the lowest extreme tide (LET) occurred on January 1st, 1987 at 22:00 and January 2nd, 1987 at 6:00,
225 respectively with the tide 1.304 m above MSL and 1.165 m below MSL. We then conduct storm surge simulations
226 at these two selected extreme tidal levels by moving the typhoon landfall time from 13:00 (UTC+8), Aug 23, 2017
227 to January 1st, 1987 at 22:00 and January 2nd, 1987 at 6:00 local time.

228 Figure 7 shows the maximum inundation maps for the real case (benchmark scenario, Figure 7a), at HET (Figure
229 7b) and LET (Figure 7c), respectively. The striking observation is that Typhoon Hato would cause inundation in
230 Macau at all the considered tidal levels (Figure 7a-c). Even Typhoon Hato occurred during the LET, the Inner
231 Harbor area would still be inundated with the maximum inundation depth up to 1.0 m (Figure 7c). We emphasize
232 here, as the LET is a representative value of the lowest extreme tidal level in the past 54 years (1964-2017), which

233   suggests the Inner Harbor area will certainly be inundated during Hato-like events regardless of the tidal levels at the
234   landfall time. The results once again highlighted the vulnerability of the Inner Harbor area to extreme flooding and
235   urgency of establishing effective protection system. Not surprisingly, if Hato had occurred at HET, a noticeably
236   greater inundation depth (0.5-0.8 m deeper in the Inner Harbor, see Figure 8) would have been sustained in all the
237   flooded areas on the Macau Peninsula with inundation extending considerably to previously unaffected areas. For
238   example, had Hato struck at the HET, the northeast Macau Peninsula, the coastal area of Taipa and Cotai would be
239   inundated with up to 1-m water depth or higher.

240   **4.3 Investigation sea level rise**

241   To account for the effects of future sea level rise (SLR), the values of 0.5 m and 1 m SLR were chosen to represent
242   the sea levels by the mid-century and end of this century based on projected local sea level rises of 30-51 cm by
243   2060 and 65-118 cm by 2100 (Wang et al., 2016). We then ran the storm surge simulations at HET and LET with
244   different magnitude of SLR 0.5 m and 1.0 m. For each simulation, we obtain the maximum inundation depths at all
245   in-land computational nodes by subtracting the DEM data from the simulated maximum wave heights. In total, we
246   derive three sets of inundation maps at current sea level, 0.5 m and 1.0 m SLR condition.

247   Adding the effect of 0.5-m and 1-m SLR at HET, the inundation extent quickly expands into the eastern part of the
248   Macau Peninsula and coastal areas of Taipa, Cotai and University of Macau, where no or limited flood was observed
249   during Typhoon Hato (Figure 9a-b). Compared with the benchmark scenario (Figure 7a), the maximum inundation
250   depths in inner harbour area will increase more than 1-1.2 m in the 0.5-m SLR scenario (Figure 9e) and 1.2-1.5 m in
251   the 1-m SLR scenario for most of the inner harbour area (Figure 9i); such increase is generally a linear combination
252   of increased tidal level and SLR. While in the eastern side of Macau Peninsula and some places in Taipa and Cotai,
253   we observe larger increases in the water depths than in the inner harbour area. The increased water depths can be up
254   to 1.2-1.5 m and 1.5-2.0 m at 0.5-m and 1-m SLR conditions, respectively. The larger increase can be partly
255   attributed to large waves in the eastern side of Macau Peninsula, coastal areas of Taipa and Cotai than in the inner
256   harbour area, especially at higher sea level conditions (Figure 10). Such spatially non-uniform response of storm
257   waves to SLR has been discussed in previous studies in many coastal areas worldwide (e.g. Atkinson et al.,
258   2013;Bilskie et al., 2016;Mcinnes et al., 2003) and China (e.g. Wang et al., 2012;Yin et al., 2017). Comparing the
259   maximum inundation depth between scenarios at LET under different sea level conditions (Figure 9c-d), we point
260   out once again that the Inner Harbor area will suffer increasingly more hazardous inundation with the rising sea
261   level. Thus engineer measures are urgently required to protect this area. When designing such engineer measures,
262   proactive policies and adaptive strategies should be taken to combat the likelihood of worsening flooding in future.

263   **5 Conclusions**

264   Typhoon Hato was one of the most damaging natural disaster events in the Western Pacific region in 2017. It caused
265   extensive coastal inundation in and around the Pearl River Delta region. In this paper, we have presented a detailed

266   post-typhoon field survey, yielding 278 measurements of maximum water depths and inundation extent on Macau
267   Peninsula. Using these data, a high-resolution flood map has been produced. These survey data have been used to
268   successfully validate a numerical model package, which consists of a WRF model for calculating the wind and
269   atmospheric pressure field and a tide-surge-wave coupled hydrodynamic model, SCHISM, for computing tides,
270   storm surges and ocean waves driven by the WRF model results. The data-model comparisons show that the skills of
271   the numerical model package are high and can capture all key features of this event, including the wind fields, the
272   water levels associated with storm surges and tides in the PRE, and the inundation depths in Macau. More
273   importantly, the numerical model package can provide additional information such as the arrival times of the storm
274   surge front and the corresponding shoreline movements.

275   The numerical model package can also be used to gain better understanding of the relative importance of different
276   causes for coastal flooding. To demonstrate this capability, we have focused on studying the effects of tidal level
277   and SLR on coastal inundation in Macau, using Typhoon Hato's atmospheric condition as a benchmark scenario..
278   One of the important observations is that regardless the tidal level during Typhoon Hato's landfall, the Inner Harbor
279   area will always be inundated with the maximum inundation depth up to 0.5 -1.0 m. On the other hand, although
280   Typhoon Hato broke all the historical records in terms of storm surge heights and flooded area, much worse scenario
281   could be expected if Typhoon Hato had occurred at a higher tidal level, and thus, caution is required if Typhoon
282   Hato is to be used as the worst-case scenario for designing future coastal defense measures. This is especially true
283   when taking the rising sea level into consideration as 0.5-m and 1-m SLR could significantly increase the severity of
284   the resulting inundation for most of the territory in Macau, including both the high tide and low tide conditions. The
285   inundation maps presented in this study provide the lower and upper bound of potential impacts of Hato-like events
286   at different tidal levels and sea level conditions. Such maps could aid the local government to make more
287   informative decisions.

288   Besides the tidal level, other factors including the landing location, track azimuth, forward speed, the sudden
289   intensification and urban development (e.g. land reclamation) may play more important role in contributing to this
290   record-breaking flood in Macau. The effects of such factors are being analyzed in more detail in a future paper.

291   Hato-like typhoon events pose a clear and significant threat to the emerging mega-cities area of the PRD and the
292   drive to expand towards the sea with extensive land reclamation and infrastructure development needed to meet the
293   demands of the growing population and the booming economy. Although most major cities in the region are
294   protected by seawalls, the protection standards vary considerably and whether such standards are sufficient to
295   combat increasingly frequent flooding in future needs careful investigation. Adaptive strategies and sustainable
296   management are almost certainly required in order to keep up with the pace of rising sea level. We believe that the
297   data and findings provided in this paper and the numerical model package will not only be of great interest to coastal
298   hazard researchers, but also to a range of stakeholders such as policy makers, town planners, emergency services
299   and insurance companies who are working to create or insure safer coastlines.

Acknowledgments, Samples, and Data

We are very grateful to the Macau people for the extremely helpful information, photographs, video footages provided, and the kindness they have shown us during the field survey. We thank Dr. Hoi Ka In for the tide data analysis and Dr Zhiguo Ma for helping processing the topographic data of Macau. We thank the Macau Meteorological and Geophysical Bureau for providing us with the meteorological data of Macau. This study is supported by AXA Research Fund Post-Doctoral Fellowship under the project "Probabilistic assessment of multiple coastal flooding hazards in the South China Sea under changing climate" to Linlin Li and the Ng Teng Fong Charitable Foundation (Hong Kong) under the joint research project "The impact of climate changes on coastal flooding hazard in South and East China Seas" between National University of Singapore and Tsinghua University. Adam Switzer was supported by (AcRF) Complexity Tier 1 Project RGC4/14 "Preparing Asian mega cities for changing climate and the potential Increase in extreme sea levels and storm surges". This paper contributes to IGCP639 "Sea level change: from Minutes to Millennia". The navigational charts in the Pearl River Estuary are purchased from Beijing Situo Ocean Information Technology Co Ltd. The topographic data of Macau was purchased from the Macau Cartography and Cadastre Bureau. The GEBCO data used in this study is downloaded from http://www.gebco.net in October 2014.

References

Atkinson, J., McKee Smith, J., and Bender, C.: Sea-Level Rise Effects on Storm Surge and Nearshore Waves on the Texas Coast: Influence of Landscape and Storm Characteristics, Journal of Waterway, Port, Coastal, and Ocean Engineering, 139, 98-117, 10.1061/(ASCE)WW.1943-5460.0000187, 2013.

Benfield, A.: Weather, Climate & Catastrophe Insight 2017 Annual Report, Aon Benfield, https://reliefweb.int/sites/reliefweb.int/files/resources/20180124-ab-if-annual-report-weather-climate-2017.pdf, 2018.

Bilskie, M. V., Hagen, S. C., Alizad, K., Medeiros, S. C., Passeri, D. L., Needham, H. F., and Cox, A.: Dynamic simulation and numerical analysis of hurricane storm surge under sea level rise with geomorphologic changes along the northern Gulf of Mexico, Earth's Future, 4, 177-193, doi:10.1002/2015EF000347, 2016.

Egbert, G. D., and Erofeeva, S. Y.: Efficient Inverse Modeling of Barotropic Ocean Tides, Journal of Atmospheric and Oceanic Technology, 19, 183-204, 10.1175/1520-0426(2002)019<0183:EIMOBO>2.0.CO;2, 2002.

ESCAP/WMO Typhoon Committee, C.: Member Report, http://www.typhooncommittee.org/12IWS/docs/Members/China20171026_final.pdf, 2017.

Fritz, H., C., B. J., E., S. C., and Jeseon, Y.: 2004 Indian Ocean tsunami flow velocity measurements from survivor videos, Geophysical Research Letters, 33, doi:10.1029/2006GL026784, 2006.

Fritz, H. M., Blount, C., Sokoloski, R., Singleton, J., Fuggle, A., McAdoo, B. G., Moore, A., Grass, C., and Tate, B.: Hurricane Katrina storm surge distribution and field observations on the Mississippi Barrier Islands, Estuarine, Coastal and Shelf Science, 74, 12-20, https://doi.org/10.1016/j.ecss.2007.03.015, 2007.

Garzon, J., and Ferreira, C.: Storm Surge Modeling in Large Estuaries: Sensitivity Analyses to Parameters and Physical Processes in the Chesapeake Bay, Journal of Marine Science and Engineering, 4, 45, 2016.

HKO: Super Typhoon Hato (1713), Hong Kong Observatory, http://www.weather.gov.hk/informtc/hato17/report.htm, 2017.

Hong, S.-Y., Dudhia, J., and Chen, S.-H.: A Revised Approach to Ice Microphysical Processes for the Bulk Parameterization of Clouds and Precipitation, Monthly Weather Review, 132, 103-120, 10.1175/1520-0493(2004)132<0103:ARATIM>2.0.CO;2, 2004.

Hong, S.-Y., Noh, Y., and Dudhia, J.: A New Vertical Diffusion Package with an Explicit Treatment of Entrainment Processes, Monthly Weather Review, 134, 2318-2341, 10.1175/mwr3199.1, 2006.

343 Iacono, M. J., Delamere, J. S., Mlawer, E. J., Shephard, M. W., Clough, S. A., and Collins, W. D.: Radiative forcing
344 by long-lived greenhouse gases: Calculations with the AER radiative transfer models, Journal of Geophysical
345 Research: Atmospheres, 113, doi:10.1029/2008JD009944, 2008.
346 Jiang, S., Xu, F., Li, Y., Liu, X., Zhao, Y., and Xu, W.: Distributional characteristics of grain sizes of surface
347 sediments in the Zhujiang River Estuary, 30-36 pp., 2014.
348 Jiménez, P. A., Dudhia, J., González-Rouco, J. F., Navarro, J., Montávez, J. P., and García-Bustamante, E.: A
349 Revised Scheme for the WRF Surface Layer Formulation, Monthly Weather Review, 140, 898-918, 10.1175/mwr-d-
350 11-00056.1, 2012.
351 Kain, J. S.: The Kain–Fritsch Convective Parameterization: An Update, Journal of Applied Meteorology, 43, 170-
352 181, 10.1175/1520-0450(2004)043<0170:TKCPAU>2.0.CO;2, 2004.
353 Krien, Y., Testut, L., Islam, A. K. M. S., Bertin, X., Durand, F., Mayet, C., Tazkia, A. R., Becker, M., Calmant, S.,
354 Papa, F., Ballu, V., Shum, C. K., and Khan, Z. H.: Towards improved storm surge models in the northern Bay of
355 Bengal, Continental Shelf Research, 135, 58-73, https://doi.org/10.1016/j.csr.2017.01.014, 2017.
356 Lee, E. K. S., Fok, L., and Lee, H. F.: An Evaluation of Hong Kong's Tropical Cyclone Warning System, Asian
357 Geographer, 29, 131-144, 10.1080/10225706.2012.742619, 2012.
358 Ma, L.-M., and Tan, Z.-M.: Improving the behavior of the cumulus parameterization for tropical cyclone prediction:
359 Convection trigger, Atmospheric Research, 92, 190-211, https://doi.org/10.1016/j.atmosres.2008.09.022, 2009.
360 Martyr, R. C., Dietrich, J. C., Westerink, J. J., Kerr, P. C., Dawson, C., Smith, J. M., Pourtaheri, H., Powell, N.,
361 Ledden, M. V., Tanaka, S., Roberts, H. J., Westerink, H. J., and Westerink, L. G.: Simulating Hurricane Storm
362 Surge in the Lower Mississippi River under Varying Flow Conditions, Journal of Hydraulic Engineering, 139, 492-
363 501, doi:10.1061/(ASCE)HY.1943-7900.0000699, 2013.
364 Mcinnes, K. L., Walsh, K. J. E., Hubbert, G. D., and Beer, T.: Impact of Sea-level Rise and Storm Surges on a
365 Coastal Community, Natural Hazards, 30, 187-207, 10.1023/a:1026118417752, 2003.
366 Pond, S., and Pickard, G. L.: Introductory Dynamical Oceanography, Oxford : Elsevier Butterworth-Heinemann,
367 1998.
368 Roland, A.: Development of WWM II: Spectral wave modeling on unstructured meshes, 2008.
369 Shan, C., Zhang, X., Yuan, H., Qian, C., Huang, X., Jiang, X., Shen, H., Sun, S., Ji, Y., Li, J., Wang, C., Zhang, Y.,
370 Zhang, B., Zheng, J., Fu, M., and Qin, X.: The hazard assessment of Typhoon Hato in Macau, China National
371 Commission for Disaster Reduction, http://www.gep.gov.mo/event/pdf/reportCN_201803.pdf, 2018.
372 Skamarock, W. C., Klemp, J. B., Dudhia, J., Gill, D. O., Barker, D., Duda, M. G., Huang, X.-y., Wang, W., and
373 Powers, J. G.: A Description of the Advanced Research WRF Version 3, National Center for Atmospheric Research,
374 Boulder, Colorado, USA, NCAR TECHNICAL NOTE, 2008.
375 SMG: Typhoon   Hato   (1713),   Macau   Meteorological   and   Geophysical   Bureau,
376 http://www.smg.gov.mo/smg/database/pdf/typhoon/e_1713.pdf, 2017.
377 Soria, J. L. A., Switzer, A. D., Villanoy, C. L., Fritz, H. M., Bilgera, P. H. T., Cabrera, O. C., Siringan, F. P., Maria,
378 Y. Y.-S., Ramos, R. D., and Fernandez, I. Q.: Repeat Storm Surge Disasters of Typhoon Haiyan and Its 1897
379 Predecessor in the Philippines, Bulletin of the American Meteorological Society, 97, 31-48, 10.1175/bams-d-14-
380 00245.1, 2016.
381 Tajima, Y., Yasuda, T., Pacheco, B. M., Cruz, E. C., Kawasaki, K., Nobuoka, H., Miyamoto, M., Asano, Y.,
382 Arikawa, T., Ortigas, N. M., Aquino, R., Mata, W., Valdez, J., and Briones, F.: Initial Report of JSCE-PICE Joint
383 Survey on the Storm Surge Disaster Caused by Typhoon Haiyan, Coastal Engineering Journal, 56, 1450006,
384 10.1142/s0578563414500065, 2014.
385 Takagi, H., Esteban, M., Shibayama, T., Mikami, T., Matsumaru, R., Leon, M. D., N.D.Thao, Oyama, T., and
386 Nakamura, R.: Track analysis, simulation, and field survey of the 2013 Typhoon Haiyan storm surge, Journal of
387 Flood Risk Management, 10, 42-52, doi:10.1111/jfr3.12136, 2017.
388 Takagi, H., Xiong, Y., and Furukawa, F.: Track analysis and storm surge investigation of 2017 Typhoon Hato: were
389 the warning signals issued in Macau and Hong Kong timed appropriately?, Georisk: Assessment and Management
390 of Risk for Engineered Systems and Geohazards, 1-11, 10.1080/17499518.2018.1465573, 2018.
391 Tewari, M., Chen, F., Wang, W., Dudhia, J., Lemone, M., Mitchell, K., Ek, M., Gayno, G., Wegiel, J., and Cuenca,
392 R.: Implementation and verification of the unified Noah land-surface model in the WRF model 20th Conference on
393 Weather Analysis and Forecasting/16th Conference on Numerical Weather Prediction, Seattle, WA, US, 2004.
394 Wang, H., Loftis, J., Liu, Z., Forrest, D., and Zhang, J.: The Storm Surge and Sub-Grid Inundation Modeling in New
395 York City during Hurricane Sandy, Journal of Marine Science and Engineering, 2, 226, 2014.
396 Wang, J., Gao, W., Xu, S., and Yu, L.: Evaluation of the combined risk of sea level rise, land subsidence, and storm
397 surges on the coastal areas of Shanghai, China, Climatic Change, 115, 537-558, 10.1007/s10584-012-0468-7, 2012.

398   Wang, L., Huang, G., Zhou, W., and Chen, W.: Historical change and future scenarios of sea level rise in Macau and
399   adjacent waters, Advances in Atmospheric Sciences, 33, 462-475, 10.1007/s00376-015-5047-1, 2016.
400   Yin, K., Xu, S., Huang, W., and Xie, Y.: Effects of sea level rise and typhoon intensity on storm surge and waves in
401   Pearl River Estuary, Ocean Engineering, 136, 80-93, https://doi.org/10.1016/j.oceaneng.2017.03.016, 2017.
402   Zhang, Y. J., and Baptista, A. M.: An Efficient and Robust Tsunami Model on Unstructured Grids. Part I:
403   Inundation Benchmarks, Pure and Applied Geophysics, 165, 2229-2248, 10.1007/s00024-008-0424-7, 2008.
404   Zhang, Y. J., Ye, F., Stanev, E. V., and Grashorn, S.: Seamless cross-scale modeling with SCHISM, Ocean
405   Modelling, 102, 64-81, https://doi.org/10.1016/j.ocemod.2016.05.002, 2016.

406

407

408
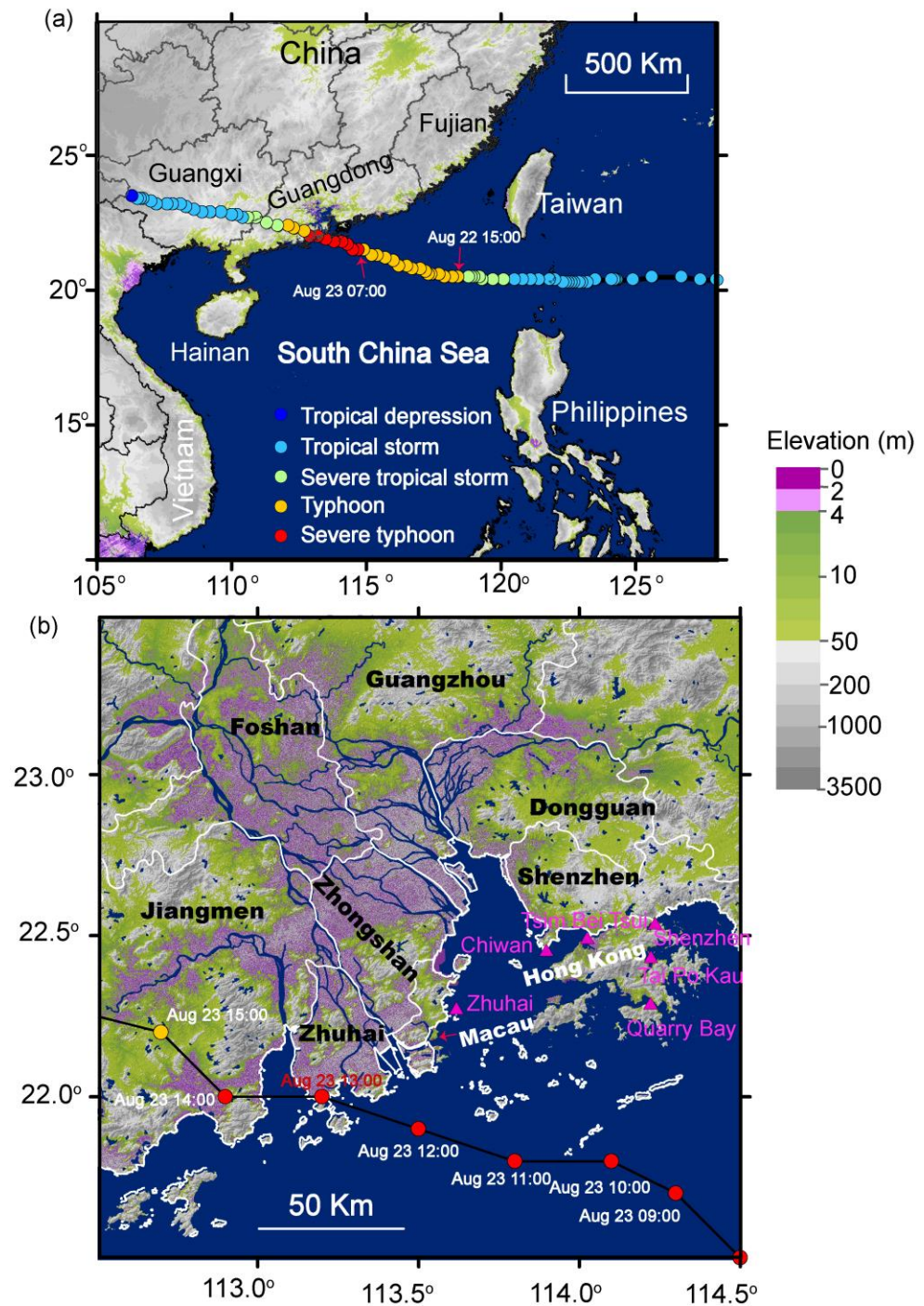
Figure 1. Typhoon Hato track data from the Chinese typhoon weather website (http://typhoon.weather.com.cn/). (a)
Typhoon Hato took a path extremely dangerous to the Pearl River Delta. It became a typhoon inside the South China
Sea at 15:00 on August 22, 2017 (local time) and further was intensified into a Severe Typhoon at 07:00 AM on
August 23 before making landfall at 12:50 PM in southern part of Zhuhai, China. (b) A close-up shows the landfall

413   location and the affected cities in the Pearl River Delta. Purple colors denote land elevation lower than 4 m above

414   mean sea level.

415

Longitude: 113.540481   Longitude: 113.53676   Longitude: 113.536548   Longitude: 113.536638
Latitude: 22.202719   Latitude: 22.199813   Latitude: 22.198702   Latitude: 22.19873

Longitude: 113.536192   Longitude: 113.5339   Longitude: 113.5368   Longitude: 113.538539
Latitude: 22.194345   Latitude: 22.18999   Latitude: 22.196137   Latitude: 22.194066

416

417   **Figure 2.** Photos taken during the field survey on the Macau Peninsula.

418
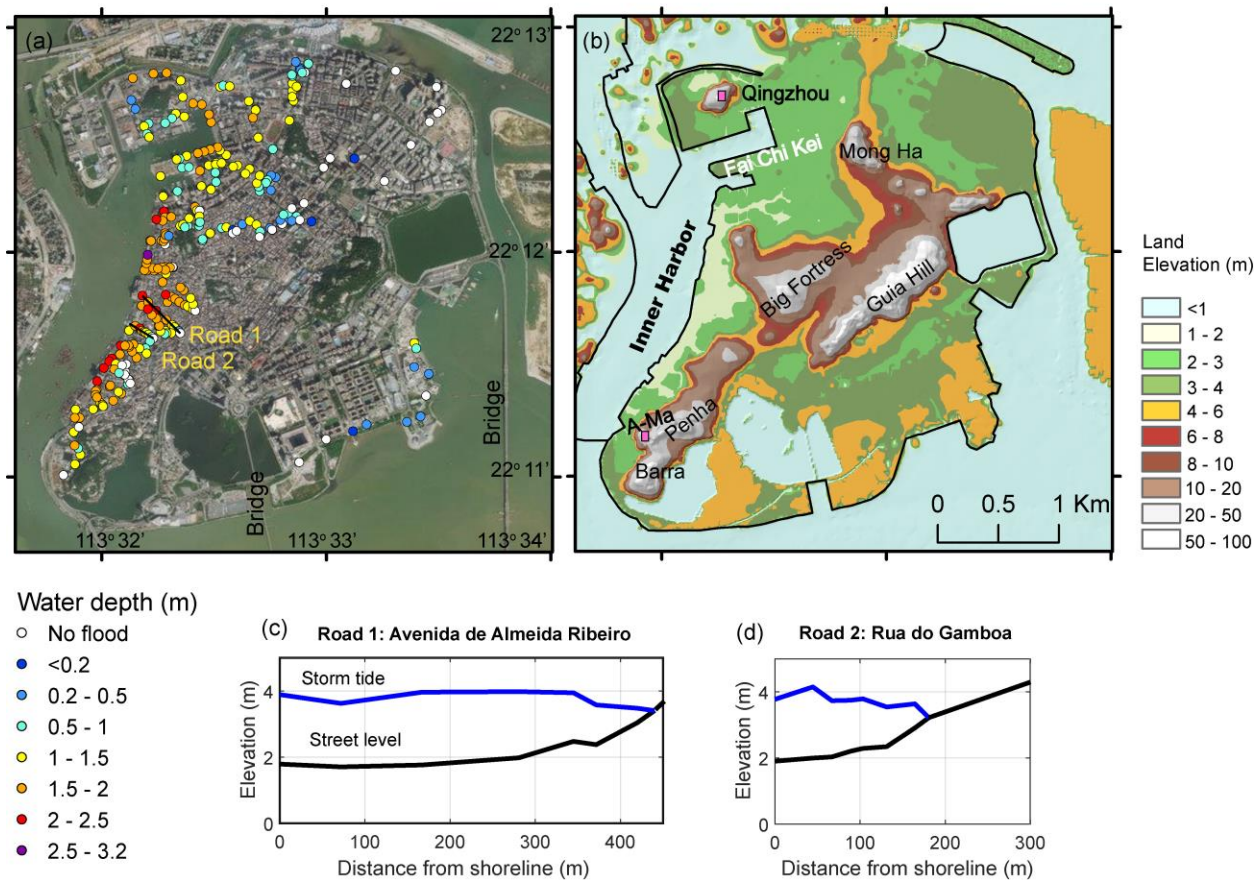
Figure 3. (a) Measured inundation depths on the Macau Peninsula shown on a Google Earth image. (b) High-resolution bare ground elevation with marked locations. (c) and (d) Profiles of surveyed inundation water depths along two main roads: Avenida de Almeida Ribeiro and Rua do Gamboa.

424
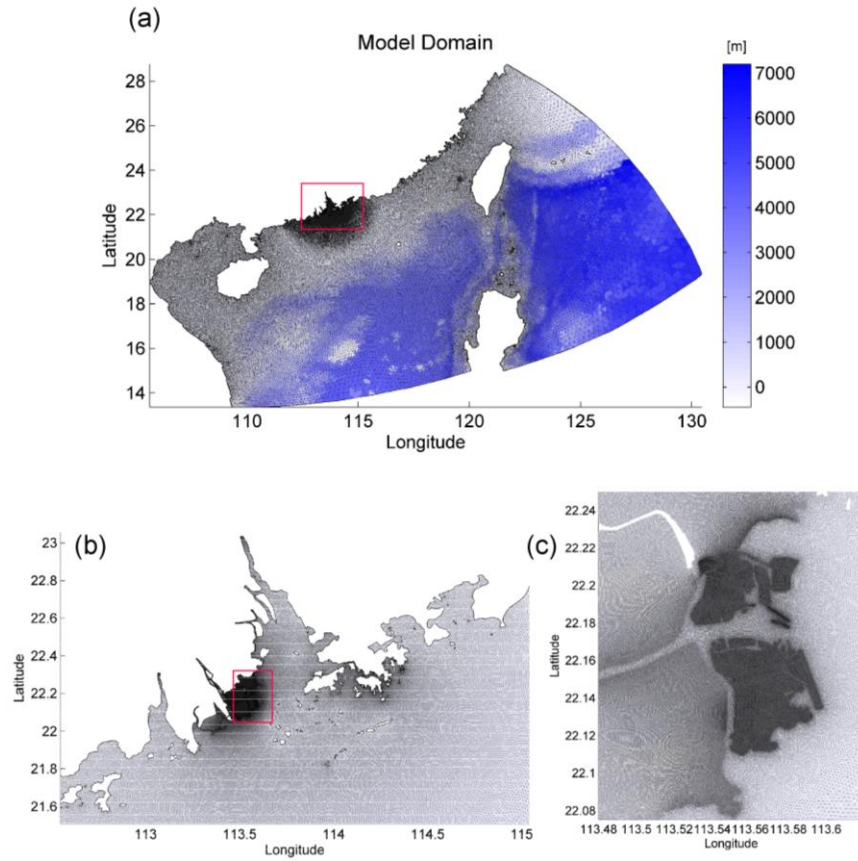
425   **Figure 4.** (a) The numerical simulation domain for SCHISM-WWMIII with close-ups showing (b) the mesh in PRD

426   and (c) the mesh near Macau.

427

428
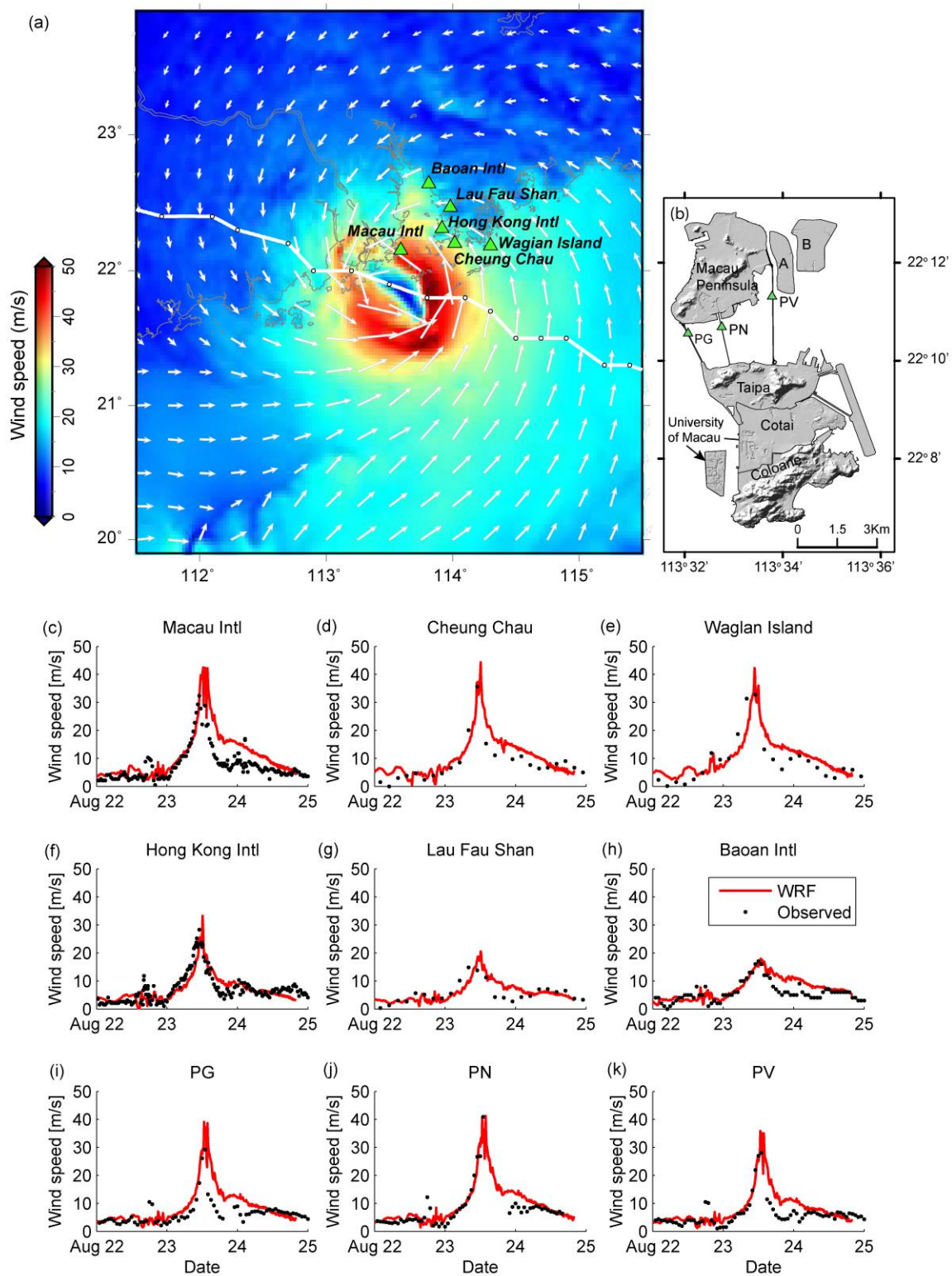
429 **Figure 5.** Wind fields generated by the WRF model: (a) In the Pearl River Estuary at 12:50 PM on August 23; (b)
430 The wind gauge locations of PG, PN and PV in Macau; (c) – (k) Comparisons of numerical results (WRF) with
431 measured wind speed at different locations. Locations and names of wind gauges (c) - (h) are shown in Figure 5a.

432
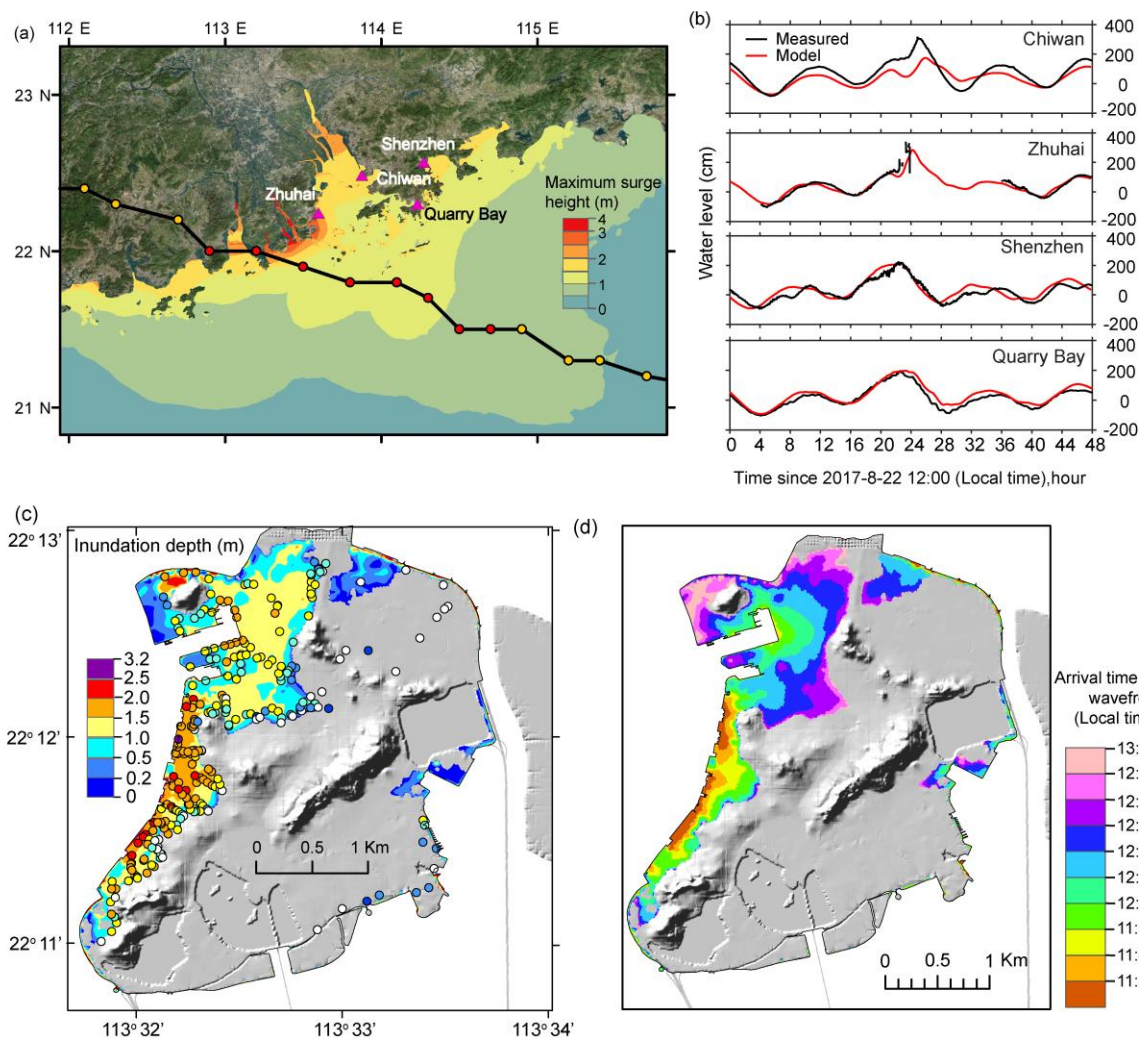
433 **Figure 6.** Numerical results capture well the key features of storm flooding induced by Typhoon Hato. (a) The
434 simulated maximum surge height in the PRE; (b) A comparison of simulated and measured storm tide at four
435 selected tide locations (marked with the green dots in Figure 5a). Note the measured data at Zhuhai station is not
436 complete due to a power cut; (c) The surveyed inundation depths (the colored dots) overlaid on the simulated
437 maximum inundation depths in the Macau Peninsula; (d) The arrival time of the flood wavefront.

438
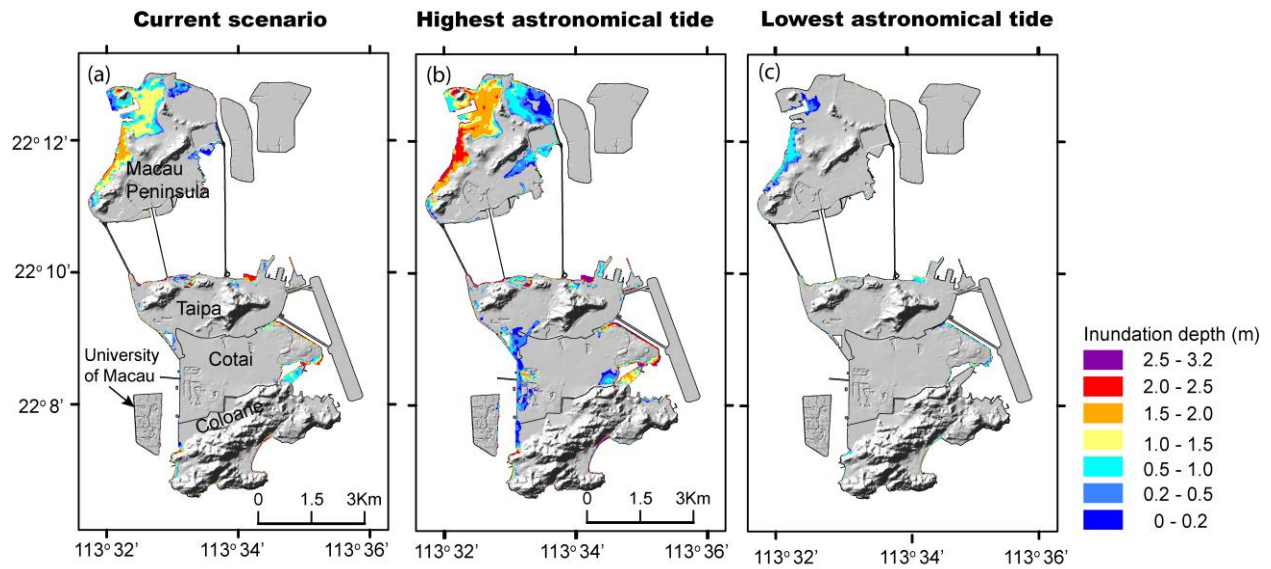
Figure 7. Maximum inundation depths for (a) the benchmark scenario; (b) the highest extreme tide and (c) the lowest extreme tide under the current sea level.

441
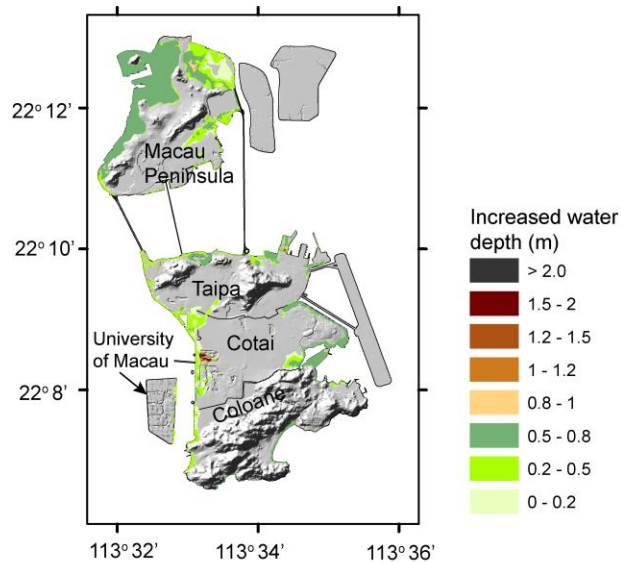
Figure 8. A map showing the difference between the maximum inundation during the benchmark scenario (Figure 5a) and the highest extreme tide under the current sea level.

444

445
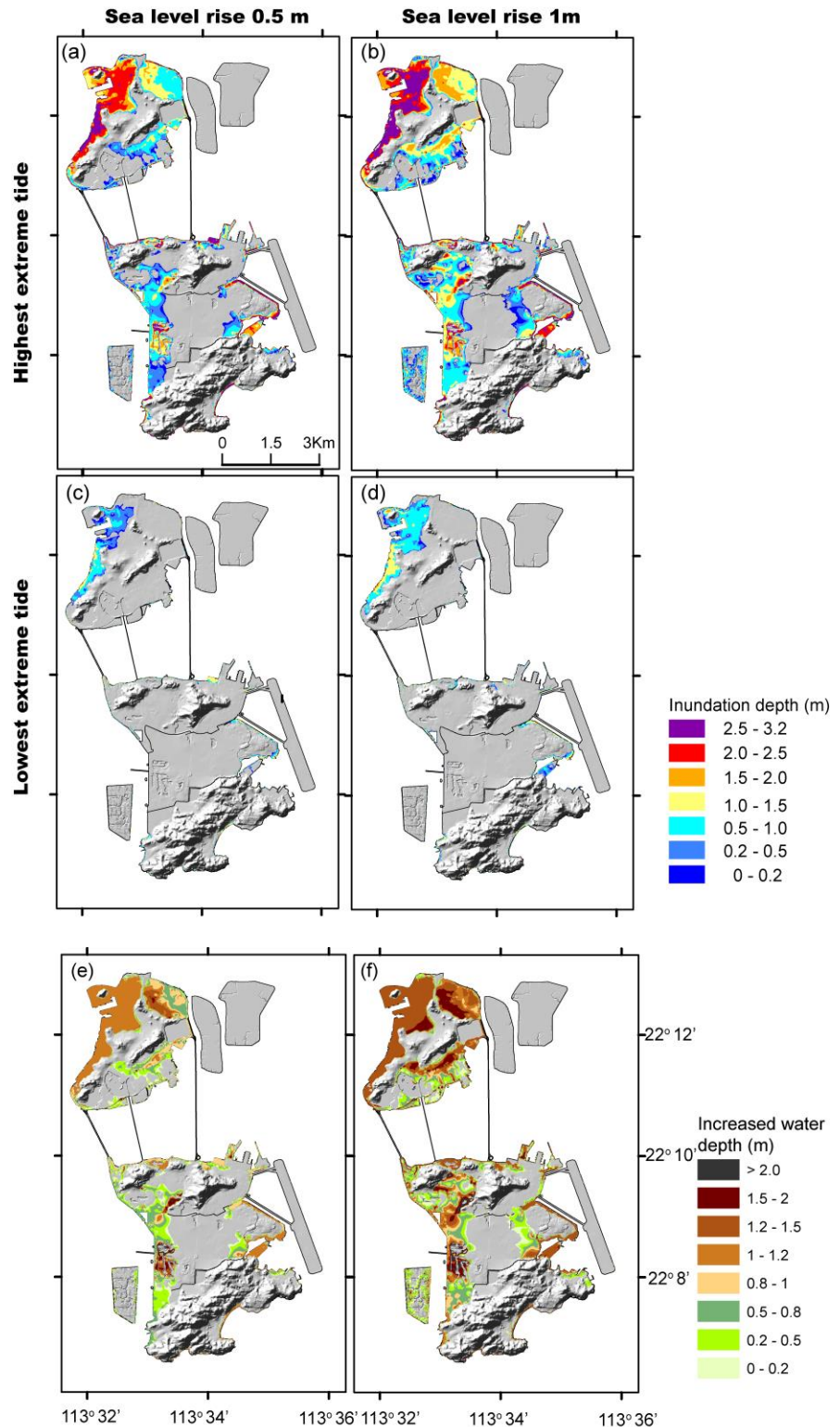
Figure 9. Maximum inundation depths during the highest extreme tide under (a) 0.5-m SLR and (b) 1-m SLR. Maximum inundation depth during the lowest extreme tide under (c) 0.5-m SLR and (d) 1-m SLR; A map showing

448   the difference between the maximum inundation during the benchmark scenario (Figure 7a) and the highest

449   extreme tide under (e) 0.5-m SLR and (f) 1-m SLR.

450

451
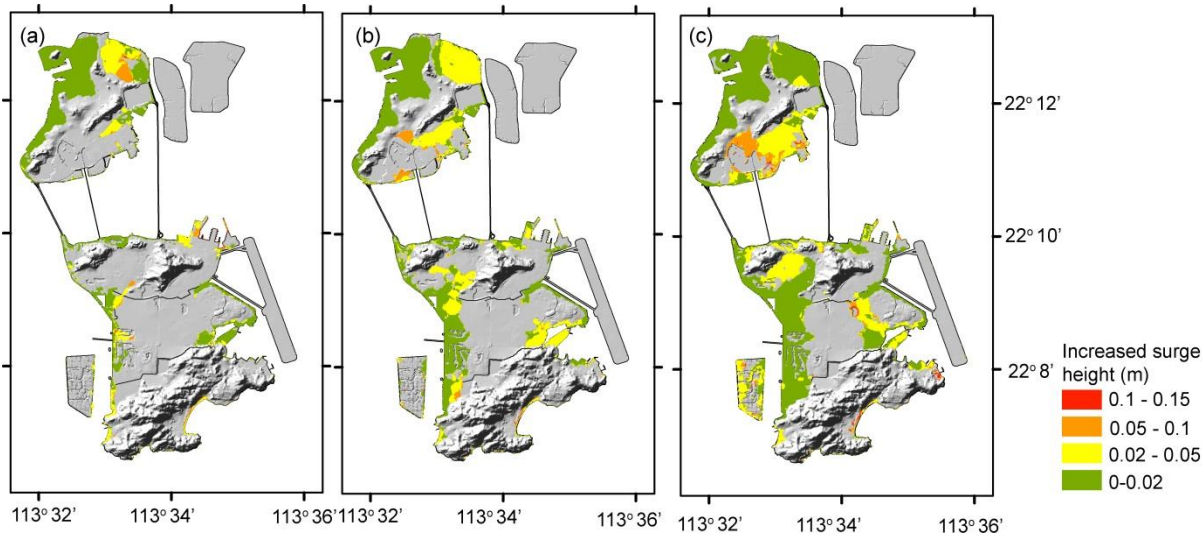
452   **Figure 10.** The difference in maximum inundation depths between scenarios with and without the wave model

453   during the highest extreme tide under (a) the current sea level (b) 0.5-m SLR, and (c) 1-m SLR.